

BIPOLAR OUTFLOW IN B335: THE SMALL-SCALE STRUCTURE¹

NAOMI HIRANO,² OSAMU KAMEYA,³ TAKASHI KASUGA,⁴ AND TOMOFUMI UMEMOTO⁵

Received 1992 January 2; accepted 1992 February 20

ABSTRACT

Interferometric observations of the ¹²CO ($J = 1-0$) and 2.6 mm continuum emission toward the young stellar object in B335 are presented. Our angular resolution of $8'' \times 5''$ is a factor of 3 higher than those of the previous single-dish observations. The ¹²CO high-velocity emission shows distinct biconical outflow structure having a size of a few thousand AU. The north-south extent of the outflow at its center is smaller than our present beam size, indicating that the outflow is focused within ~ 1000 AU of its origin. Within $\sim 4''$ of the outflow center, there is a 2.6 mm continuum source with a peak flux of ~ 80 mJy. This indicates that the very dense material of $n(\text{H}_2) \gtrsim 10^8 \text{ cm}^{-3}$ is surrounding the young stellar object which should be the driving source of the outflow. Such dense material may be responsible for collimating the outflow into two oppositely directed jets. In the vicinity of the origin, the outflow shows a sudden increase in velocity away from its center. A simple dynamical model of the expanding “snowplowing” shell can explain the velocity field of the outflow in B335.

Subject headings: ISM: individual objects (B335) — ISM: jets and outflows — ISM: molecules — stars: formation

1. INTRODUCTION

The bipolar outflow in the small dark cloud B335 is one of the best studied examples of the low-mass star-forming regions. The proximity of B335 to the Sun (250 pc; Tomita, Saito, & Ohtani 1979), isolation from other star-forming region, and quiet kinematics of the ambient molecular cloud allow us to study the intrinsic properties of the molecular outflow. The high-resolution maps of ¹²CO ($J = 1-0$) (Goldsmith et al. 1984; Hirano et al. 1988; Cabrit, Goldsmith, & Snell 1988; Moriarty-Schieven & Snell 1989) show that the outflow is of biconical shape with a constant opening angle of $\sim 45^\circ$ and is centered at the low-luminosity far-infrared source, IRAS 19347+0727. Furthermore, B335 is the most suitable object to study the detailed structure of the outflow because its axis has a small inclination angle to the plane of the sky, $\sim 10^\circ$ (Hirano et al. 1988; Cabrit et al. 1988; Moriarty-Schieven & Snell 1989). Hirano et al. (1988) have detected strong high-velocity ¹²CO emission toward the IRAS source, which has never been known. The N–S extent of the outflow is not resolved with $16''$ beam at the position of the IRAS source. These results strongly suggest that the outflow is currently active and is focused within 4000 AU ($\sim 6 \times 10^{16}$ cm) of its driving source. The small scale structure of the outflow adjacent to its origin is interesting because it is the clue to the collimation and driving mechanism of the molecular outflow.

In this *Letter*, we present the first interferometric maps of the ¹²CO ($J = 1-0$) and 2.6 mm continuum emission of the outflow source, B335. Our angular resolution of $8'' \times 5''$ corre-

sponds to the linear scale of 2000×1200 AU. This resolution is at least a factor of 3 higher than those of the previous single-dish observations. The main purposes of this work are to know (1) in what scale the outflow is collimated, (2) how are the structure and velocity field of the outflow, and (3) what is the relationship between the outflow and the dense core or disk surrounding the young stellar object.

2. OBSERVATIONS

Observations were made on 1988 December 14, 1989 January 30, and 1989 May 24 using the Nobeyama Millimeter Array. The primary beam size was $65''$ in HPBW. Two configurations of five 10 m antennas gave 20 independent baselines. The synthesized beam had a size of $8.1'' \times 5.0''$ (HPBW) with a position angle of 153.7° . The field center was the position of IRAS 19345+0727, $\alpha = 19^{\text{h}}34^{\text{m}}35^{\text{s}}.3$, $\delta = +7^{\circ}27'24''$ (1950). All the antennas were equipped with SIS receivers whose system temperatures (SSB) were ~ 600 K at 115 GHz. The backend was a 1024 channel digital FFT spectro-correlator. The bandwidth was 320 MHz and the frequency resolution was 312 kHz. The frequency resolution corresponds to 0.81 km s^{-1} at 115 GHz.

For visibility calibration, IRAS 2145+067 was observed every 30 minutes. The flux density of IRAS 2145+067 was 4.2 Jy. The bandpass calibration was made from the observations of 3C 84. The observed visibility data were Fourier-transformed and CLEANed by using the Astronomical Image Processing System (AIPS), which is installed on computers of the Nobeyama Radio Observatory. We employed natural weighting to obtain maps. No zero-spacing flux was introduced. The rms noise level in the ¹²CO maps with 312 kHz resolution is $0.13 \text{ Jy beam}^{-1}$, and the rms noise in the continuum map with 320 MHz bandwidth is 15 mJy beam^{-1} .

3. RESULTS

3.1. ¹²CO Outflow

The ¹²CO emission is detected in nine FX channels whose velocity ranges are from 4.2 to 8.2 km s^{-1} and from 9.1 to 12.3

¹ Based on the observations made at the Nobeyama Radio Observatory (NRO). Nobeyama Radio Observatory is a branch of the National Astronomical Observatory, an inter-university research institute operated by the Ministry of Education, Science, and Culture, Japan.

² Laboratory of Astronomy and Geophysics, Hitotsubashi University, Kunitachi, Tokyo, 186, Japan.

³ Mizusawa Astrogeodynamics Observatory, Mizusawa, Iwate, 023, Japan.

⁴ Department of Instrument and Control Engineering, College of Engineering, Hosei University, Kajinocho, Koganei, Tokyo, 184, Japan.

⁵ Nobeyama Radio Observatory, Minamimaki, Minamisaku, Nagano, 284-13, Japan.

km s⁻¹. These velocity ranges correspond to those of the blueshifted and redshifted molecular outflow detected by single-dish observations (Goldsmith et al. 1984; Hirano et al. 1988; Cabrit et al. 1988; Moriarty-Schieven & Snell 1989). This indicates that the ¹²CO emission detected by the interferometer is the wing emission which originates from the outflowing gas. The total integrated flux of the blueshifted ($V_{\text{LSR}} = 4.2\text{--}8.2$ km s⁻¹) ¹²CO emission is 38.4 Jy km s⁻¹ and that of the redshifted ($V_{\text{LSR}} = 9.1\text{--}13.1$ km s⁻¹) one is 29.2 Jy km s⁻¹, which are about 15% and 26% of the single-dish flux obtained by the 45 m telescope, respectively.

In Figures 1a–1g, we present channel maps. The central velocity of each channel is (a) 6.22 km s⁻¹, (b) 7.03 km s⁻¹, (c) 7.84 km s⁻¹, (d) 8.65 km s⁻¹, (e) 9.46 km s⁻¹, (f) 10.28 km s⁻¹, and (g) 11.09 km s⁻¹. Figure 1d, which is a map at the line center velocity, shows no significant emission. This may be due to the fact that the ambient cloud emission is mostly resolved out. We note that no velocity component shows a centrally peaked distribution. This suggests that there is no compact and strong high-velocity component in the central region of the outflow. Both eastern and western lobes contain the blueshifted and redshifted components. This is consistent with the outflow axis being almost perpendicular to the line of sight.

Another feature of the outflow emission is the double-lobed and fan-shaped structure along the east-west direction seen in Figures 1c (blueshifted low-velocity component, hereafter referred to as BLC) and 1e (redshifted low-velocity component, RLC). These results suggest that the biconical morphology of the outflow is already settled within a few thousand AU of its origin. Two prominent peaks are separated by 10" in BLC and 15" in RLC, which correspond to 2400 AU and 3600 AU, respectively. Between two peaks, the ¹²CO intensity has a local minimum. The minimum position in BLC and that in RLC are displaced by ~3" (see Fig. 2). This can be understood if the axis of the outflow is slightly inclined relative to the plane of the sky. The N–S extent of the CO flow at the center is not

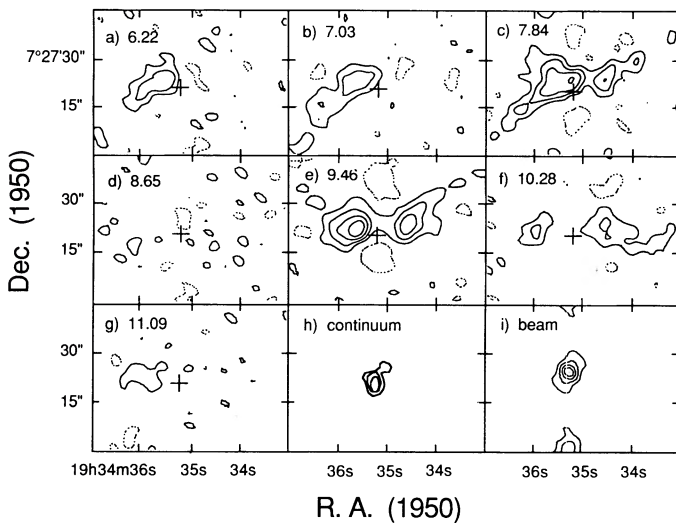


FIG. 1.—(a–g) Channel maps of the ¹²CO ($J = 1\text{--}0$) emission. The center velocity of each channel is (a) 6.22 km s⁻¹, (b) 7.03 km s⁻¹, (c) 7.84 km s⁻¹, (d) 8.65 km s⁻¹, (e) 9.46 km s⁻¹, (f) 10.28 km s⁻¹, and (g) 11.09 km s⁻¹. Contours are every 0.97 Jy beam⁻¹ (2σ) with the lowest contours of 0.97 Jy beam⁻¹. The broken contours are for negative intensities. The position of the 2.6 mm continuum peak is marked with the cross. (h) Map of 2.6 mm continuum emission. The lowest contour level is 30 mJy (2σ) and contour spacing is 15 mJy. (i) The synthesized beam is presented. Contours are every 20% of the peak.

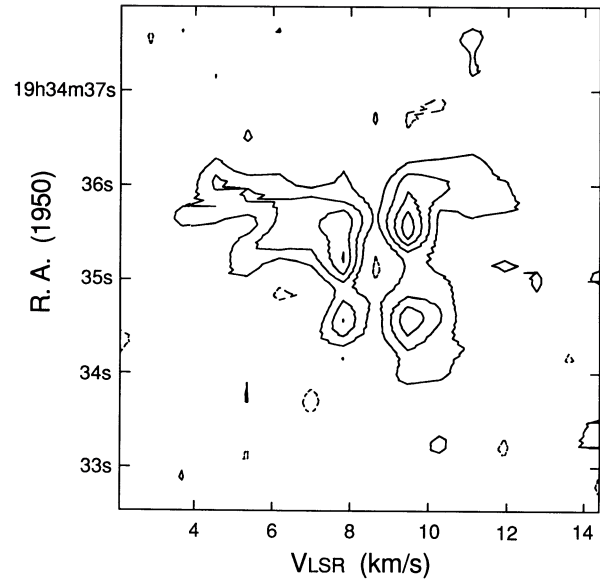


FIG. 2.—Position-velocity diagram along the east-west direction at $\delta = 7^\circ 27' 23''$. Contours are every 0.97 Jy beam⁻¹ with the lowest contours of 0.97 Jy beam⁻¹. The broken contours are for negative intensities.

resolved with our present beam, indicating that it is smaller than 8" (= 2000 AU). This suggests that the outflow is focused within ~1000 AU of its origin.

The position-velocity diagram along the east-west direction is shown in Figure 2. The gap at $V_{\text{LSR}} \sim 8.5$ km s⁻¹ corresponds to the ambient velocity component which has been resolved out. Although our velocity resolution of ~0.81 km s⁻¹ is not high enough to reveal detail of the velocity structure of B335 outflow, the position-velocity diagram shows some evidence for a velocity increase away from the center, particularly in the eastern lobe.

3.2. Energetics

We have estimated the mass of the high-velocity gas from the observed line flux by using the result of Scoville et al. (1986):

$$M = 2.19 \times 10^{-5} \frac{T_{\text{ex}} + 0.93}{\exp(-5.59/T_{\text{ex}}) (1 - e^{-\tau})} \times d_{\text{kpc}}^2 \int S_{\nu} dv M_{\odot}, \quad (1)$$

where T_{ex} is the ¹²CO excitation temperature, τ is the averaged optical depth of the ¹²CO line wings, d is the distance to B335 in kpc, and S_{ν} is the line flux density measured in Jy. We adopted an H₂ to CO abundance ratio of 10⁴ and a mean atomic weight of the gas of 1.36. We used an excitation temperature of 12 K and an averaged optical depth of ~6, which are derived from the $J = 2\text{--}1$ and $J = 1\text{--}0$ data of ¹²CO and ¹³CO (Hirano et al. 1991). The masses of the blueshifted and redshifted gas are estimated to be $6.5 \times 10^{-3} M_{\odot}$ and $4.9 \times 10^{-3} M_{\odot}$, respectively. If the distribution of the outflowing material is uniform in two lobes whose diameters are 15" (~3600 AU), the averaged molecular gas density becomes 6×10^4 cm⁻³. Averaged radial velocity v_{rad} of this compact flow component is ~1.7 km s⁻¹. After the correction of the inclination angle from the plane of the sky of ~10°, the flow velocity v_{flow} becomes ~10 km s⁻¹. The total momentum of this flow component is ~0.1 M_{\odot} km s⁻¹. The dynamical time

scale, τ_d , calculated from v_{flow} and the size of the lobe, 3600 AU, is 2×10^3 yr. This time scale is a factor of 10 smaller than that of the whole outflow region, 2×10^4 yr, estimated from the single-dish maps (Hirano et al. 1988). The mechanical luminosity, L_{mech} , and the force, F , are $0.05 L_{\odot}$ and 4×10^{26} dynes, respectively. If we consider the contribution of the missing flux, which is 3 or 4 times of that of the observed flux, L_{mech} and F are comparable to the values of Hirano et al. (1988). This result means that the outflow activity has been almost constant during its duration of 2×10^4 yr.

3.3. Continuum Emission

Figure 1h shows a map of the 2.6 mm continuum emission. The continuum emission peaks at $\alpha(1950) = 19^{\text{h}}34^{\text{m}}35^{\text{s}}.2$, $\delta(1950) = 7^{\circ}27'21''$. This position lies midway between that found by Keene et al. (1983) and that given by *IRAS*. The continuum source lies almost center of the outflow; but its peak position is $\sim 3''$ – $4''$ southeast of the outflow center.

The peak flux is ~ 80 mJy beam $^{-1}$ and the total integrated flux is 80 mJy. In Figure 3, our 2.6 mm continuum measurement is combined with the previous far-infrared and submillimeter measurements by Keene et al. (1983), Gee et al. (1985), Chandler et al. (1990) and *IRAS* (*IRAS* Point Source Catalog, Version 2, 1988). The spectral energy distribution from 100 μm to 2.6 mm wavelength is fitted with both optically thin and optically thick dust emission. An optically thin fit ($\Omega_s B_{\lambda}(T)\tau_{\lambda}$, where $B_{\lambda}(T)$ is the Planck function, Ω_s is the source size, and τ_{λ} is the dust optical depth; solid line in Fig. 3) provides $T_{\text{dust}} = 18$ K and a $\lambda^{-1.5}$ emissivity law. Assuming that the source size is same as our present beamsize, 46 arcsec 2 , the optical depth at 2.6 mm is estimated to be 0.01. On the other hand, an optically thick fit ($\Omega_s B_{\lambda}(T)[1 - \exp(-\tau_{\lambda})]$; dashed line in Fig. 3) provides $T_{\text{dust}} = 25$ K, a uniformly bright source size of 11 arcsec 2 , an optical depth at 2.6 mm of 0.02, and a λ^{-2} emissivity law.

The column density and the total mass of the gas are estimated by assuming the dust emissivity law and the relationship

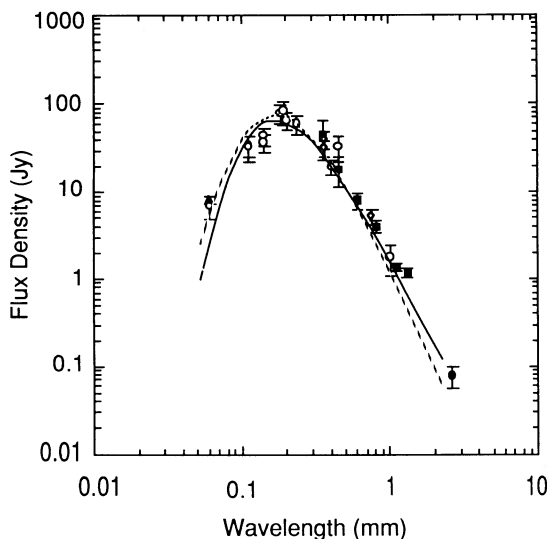


FIG. 3.—Far-infrared/submillimeter/millimeter spectrum of the continuum source of B335. Filled circles: data from this paper. Open diamonds: data from Gee et al. (1985). Filled squares: data from Chandler et al. (1990). Open circles: data from Keene et al. (1983). Filled triangles: data from the *IRAS* Point Source Catalog (Version 2, 1988). Solid curve denotes the optically thin fit, and dashed curve denotes the optically thick fit.

between 400 μm optical depth and hydrogen column density, $N(\text{H}_2)/\tau_{400\mu\text{m}} = 6 \times 10^{24} \text{ cm}^{-2}$ (Hildebrand 1983). The peak column densities are 1×10^{24} and $6 \times 10^{24} \text{ cm}^{-2}$ for $\lambda^{-1.5}$ and λ^{-2} emissivity law, respectively. The total mass of the gas estimated from the integrated flux is $1.7 M_{\odot}$ for $\lambda^{-1.5}$ emissivity law and $2.9 M_{\odot}$ for λ^{-2} emissivity law. These masses are in satisfactory agreement with those obtained by Keene et al. (1983) and Chandler et al. (1990). We can estimate the volume density of the continuum emitting region by assuming its size. If the source size is same as the beam size, $8'' \times 5''$, which corresponds to a linear size of 2000×1200 AU and the region has a cylindrical geometry of 1000 AU in radius and 1200 AU thick, the mean hydrogen number density is estimated to be $\sim 10^8 \text{ cm}^{-3}$. If the source size is 11 arcsec 2 , which is derived from an optically thick fit, the mean density becomes ~ 4 times larger than the former case.

4. DISCUSSION

4.1. Outflow Collimation

We discuss the collimation mechanism of the molecular outflow traced by the ^{12}CO emission. First, we consider the possibility of the disk-driven outflow models (e.g., Pudritz & Norman 1986 and Uchida & Shibata 1985), which predict the flows originate from radii as large as 100–1000 AU. These models require that the energy of the outflow, E_{flow} , is supplied by the rotational energy of the disk surrounding the young stellar object, E_{rot} . If the disk of 1.7 – $2.9 M_{\odot}$ and 1000 AU in radius is in Keplerian rotation around a $2 M_{\odot}$ central object, it contains the rotational energy ($E_{\text{rot}} \sim GM_{\text{disk}}M_{\star}/R_{\text{disk}}$, where R_{disk} is the disk radius, and M_{disk} and M_{\star} are the mass of the disk and the central object, respectively) of $(0.6$ – $1) \times 10^{44}$ ergs. The kinetic energy of the outflow, E_{flow} , estimated from the single-dish ^{12}CO observations of Hirano et al. (1988) is 7×10^{44} ergs. This is a factor of 7–12 larger than the disk rotational energy, indicating that the disk rotational energy is too small to drive the molecular outflow in B335. There is a possibility that the disk was more massive in the past; however, a massive disk of $\geq 10 M_{\odot}$ is unlikely because the mass of the B335 cloud is no more than 11–22 M_{\odot} (Frerking, Langer, & Wilson 1987, Martin & Barrett 1978). In addition, there is no sign of rotation in the velocity field of ^{12}CO outflow as predicted by the disk-driven outflow models.

Next we examine the possibility that the outflow is driven by the stellar wind which is intrinsically isotropic. In this case, the stellar wind should be collimated into two oppositely directed jets by the dense matter surrounding the young stellar object (e.g., Plambeck et al. 1982) and the CO outflow is a shell swept up by the stellar wind. The dynamical pressure of the steady stellar wind is given by

$$\rho_w v_w^2 = M_w v_w^2 / V_{\text{lobe}}, \quad (2)$$

where ρ_w and v_w are the average density and velocity of the stellar wind, V_{lobe} is the volume of the outflow lobes, and M_w is the mass in the wind at any time. Assuming momentum conservation, $M_w v_w^2 = M_s v_s^2$, where M_s and v_s are the mass and velocity of the swept-up shell (Snell et al. 1985), we obtain

$$\rho_w v_w^2 = M_s v_s^2 / V_{\text{lobe}}. \quad (3)$$

Using the outflow mass of $0.01 M_{\odot}$, velocity of 10 km s^{-1} , and the lobe size of ~ 3600 AU, we estimate the dynamical pressure of the stellar wind to be $\sim 3 \times 10^{-7} \text{ dynes cm}^{-2}$. If we use the single-dish results of Hirano et al. (1988), the calculated

dynamical pressure becomes a factor of ~ 20 smaller. The ambient pressure in the disk, $P_0 = n_0 k T_0$, where n_0 and T_0 are the density and temperature of the disk and k is the Boltzmann constant, is 2×10^{-7} dynes dm^{-2} for $n_0 = 10^8 \text{ cm}^{-3}$ and $T_0 = 18 \text{ K}$, and is 2×10^{-6} dynes cm^{-2} for $n_0 = 6 \times 10^8 \text{ cm}^{-3}$ and $T_0 = 25 \text{ K}$. These values are comparable to or larger than the dynamical pressure of stellar wind. Hence, a dense disk of $\gtrsim 10^8 \text{ cm}^{-3}$ can confine and channel the outflow. Thus we suggest that the outflow in B335 is more likely to be a stellar wind driven shell than a disk-driven wind.

4.2. Flow Velocity

As seen in the position-velocity diagram, the flow velocity in the vicinity of its origin suddenly increases away from its central source. Such velocity increase is easily explained in terms of a "snowplowing" shell expanding into an ambient medium with a steep density gradient.

For simplicity, we adopt a spherical symmetric geometry, that is, a spherical shell expanding into an isotropic medium. A dynamical model including the bipolar geometry is presented by Shu et al. (1991). As the shell moves outward with velocity $v_s = dr_s/dt$, the mass of the shell M_s increases as follows,

$$dM_s/dt = 4\pi r^2 \rho(r) v_s, \quad (4)$$

where $\rho(r)$ is the density of the ambient medium. If the shell is driven by the momentum of the stellar wind, the momentum equation is

$$d(M_s v_s)/dt = \dot{M}_w v_w, \quad (5)$$

where \dot{M}_w is the stellar mass-loss rate. Using equations (4), (5), and the momentum conservation equation, $\dot{M}_w v_w^2 = M_s v_s^2$, we obtain,

$$dv_s/dt = (\dot{M}_w v_w / M_s)(1 - 4\pi r^3 \rho(r) / M_s). \quad (6)$$

Assuming an ambient density distribution of the form $\rho(r) = \rho_0 r^{-\alpha}$, we find that $dv_s/dt < 0$ for $\alpha < 2$, $dv_s/dt = 0$ for $\alpha = 2$,

and $dv_s/dt > 0$ for $\alpha > 2$. This means that if the density gradient is steeper than r^{-2} , the snowplowing shell is accelerated as it moves outward. On the other hand, the shell is decelerated if the density gradient is flatter than r^{-2} . According to Hasegawa, Rogers, & Hayashi (1991), the radial density distribution in B335 follows a power law with $\alpha \cong 3$ within the region $r \lesssim 35''$. Thus, our simple analysis can explain that such a steep density gradient of $\alpha \cong 3$ is responsible for the acceleration of the outflow within the field of our observations. The high-resolution single-dish results (Hirano et al. 1992) reveal that the flow velocities reach maxima at $r \sim 30''$ and for $r \gtrsim 30''$ they are slightly decelerated. Such velocity structure is well explained by our simple model because the density-law index $\alpha \cong 0.8$ for the region of $35'' \lesssim r \lesssim 3'$ (Frerking, Langer, & Wilson 1987).

5. CONCLUSIONS

Interferometric observations provide us with a detailed view of the molecular outflow in B335. On a small scale the outflow shows a distinct biconical shape centered at the 2.6 mm continuum source. The north-south extent of the outflow at its center is not resolved by our present beam. This implies that the collimation of the outflow has occurred within $\sim 1000 \text{ AU}$ of its origin. Our 2.6 mm continuum measurements suggest that the very dense material of $\gtrsim 10^8 \text{ cm}^{-3}$ is surrounding the young stellar object which should be the driving source of the outflow. Such a high-density core or disk may be responsible for collimating the outflow into two oppositely directed jets.

A simple dynamical model of the expanding "snowplowing" shell can explain the velocity structure of the outflow; the outflow is accelerated in the region whose ambient density gradient is $\propto r^{-3}$ and is slightly decelerated where the density law is $\propto r^{-0.8}$.

We would like to thank the staff of NRO for the operation in our observations and the support in data reduction.

REFERENCES

- Cabrit, S., Goldsmith, P. F., & Snell, R. L. 1988, *ApJ*, 334, 196
 Chandler, C. J., Gear, W. K., Sandell, G., Hayashi, S., Duncan, W. D., Griffin, M. J., & Hazell, A. S. 1990, *MNRAS*, 243, 330
 Frerking, M. A., Langer, W. D., & Wilson, R. W. 1987, *ApJ*, 313, 320
 Gee, G., Griffin, M. T., Cunningham, C. T., Emerson, J. P., Ade, P. A. R., & Caroff, L. J. 1985, *MNRAS*, 215, 15
 Goldsmith, P. F., Snell, R. L., Hemeon-Heyer, M., & Langer, W. D. 1984, *ApJ*, 286, 599
 Hasegawa, T. I., Rogers, C., & Hayashi, S. S. 1991, *ApJ*, 374, 177
 Hildebrand, R. H. 1983, *QJRAS*, 24, 267
 Hirano, N., Kameya, O., Nakayama, M., & Takakubo, K. 1988, *ApJ*, 327, L69
 Hirano, N., Kameya, O., Kasuga, T., Hasegawa, T., Hayashi, S. S., & Umemoto, T. 1991, in *Molecular Clouds*, ed. R. A. James & T. J. Millar (Cambridge: Cambridge Univ. Press), 115
 Hirano, N., et al. 1992, in preparation
 IRAS Point Source Catalog, Version 2, 1988, Joint IRAS Science Working Group (Washington, DC: GPO)
 Keene, J., Davidson, J. A., Harper, D. A., Hildebrand, R. H., Jaffe, D. T., Lowenstein, R. F., Low, F. J., & Pernic, R. 1983, *ApJ*, 274, L43
 Martin, R. N., & Barrett, A. H. 1978, *ApJS*, 36, 1
 Moriarty-Schieven, G. H., & Snell, R. L. 1989, *ApJ*, 338, 952
 Plambeck, R. L., Wright, M. C. H., Welch, W. J., Bieging, J. H., Baud, B., Ho, P. T. P., & Vogel, S. N. 1982, *ApJ*, 259, 617
 Pudritz, R. E., & Norman, C. A. 1986, *ApJ*, 301, 571
 Scoville, N. Z., Sargent, A. I., Sanders, D. B., Claussen, M. J., Masson, C. R., Lo, K. Y., & Phillips, T. G. 1986, *ApJ*, 303, 416
 Shu, F. H., Ruden, S. P., Lada, C. J., & Lizano, S. 1991, *ApJ*, 370, L31
 Snell, R. L., Bally, J., Strom, S. E., & Strom, K. M. 1985, *ApJ*, 290, 587
 Tomita, Y., Saito, T., & Ohtani, H. 1979, *PASJ*, 31, 407
 Uchida, Y., & Shibata, K. 1985, *PASJ*, 37, 515